CMS Physics Analysis Summary

Contact: cms-pag-conveners-exotica@cern.ch 2017/05/15

Search for stopped long-lived particles produced in pp collisions at $\sqrt{s} = 13$ TeV

The CMS Collaboration

Abstract

A search is presented for long-lived particles that lose sufficient kinetic energy and come to rest in the CMS detector. If such a particle decays to at least one standard model particle, it would produce a spectacular signature: a high-energy jet that is not coincident with the proton-proton collisions. During the time intervals without collisions, the detector is quiet and only rare background processes must be considered. The 2015 search is performed using a 2.7 fb^{-1} sample of pp collision run data at $\sqrt{s} = 13$ TeV, corresponding to 135 hours of trigger livetime, while the 2016 search is carried out using a 36.8 fb^{-1} sample of pp collision run data at the same energy, which corresponds to 586 hours of trigger livetime. Four events are observed in the 2015 analysis and thirteen events are observed in the 2016 analysis; both observed numbers of events are consistent with the predicted backgrounds. Limits are placed on the mass of gluinos and stop quarks with lifetimes spanning 13 orders of magnitude. Assuming a cloud model of R-hadron interactions, and combining the results from the 2015 and 2016 analyses, for $E_{\mathrm{g}} > 130$ GeV and $BR(\tilde{g} \to g\tilde{\chi}^0) = 100\%$, gluinos with lifetimes from 10 μs to 1000 s and $m_{\tilde{g}} < 1385$ GeV are excluded. Under a similar assumption, $E_{\mathrm{t}} > 170$ GeV and $BR(\tilde{t} \to t\tilde{\chi}^0) = 100\%$, we are able to exclude long-lived stop quarks with lifetimes from 10 μs to 1000 s and $m_{\tilde{t}} < 744$ GeV. These are the strongest limits on stopped long-lived particles to date.

1 Introduction

Many extensions of the standard model (SM) predict the existence of new heavy long-lived particles [1–6]. At the CERN LHC the two general-purpose detectors, ATLAS and CMS, have set stringent limits on the existence of such particles with searches [7, 8] that exploit the anomalously large energy loss and/or longer time-of-flight that these particles would exhibit as they traverse the detectors. These searches are complemented by this search that targets the fraction of such particles with sufficiently low kinetic energy that they come to rest in the detectors. In this case, the subsequent decays can be directly observed, allowing the reconstruction of the "stopped" particles and the study of their characteristics.

Long-lived heavy particles, such as gluinos or stops, could be pair produced in proton-proton collisions and hadronize into R-hadrons. These R-hadrons would interact with detector material via nuclear interactions and, if charged, by ionization. Below a critical velocity, the kinetic energy of this R-hadron will go to zero so that such particle comes to rest within the detector and, at some later time, decays. Assuming at least one daughter particle is a SM particle and the R-hadron has stopped in the instrumented region of the detector, the decay should be observable. More specifically, if the stopping position is inside the calorimeter, as is most likely given its density, the experimental signature will be a randomly-timed, relatively large energy response spread over a few channels. Since these deposits might be difficult to differentiate from those of SM particles produced in pp collisions, they would be most easily observed at times between pp collisions. During these times, there are no proton collisions occurring at the center of the detector so that only cosmic rays, beam halos and instrumental noise are recorded.

This Physics Analysis Summary describes a search for such stopped particles using 2015 data with a total integrated luminosity of 2.7 fb^{-1}, as well as the 2016 data with a total integrated luminosity of 36.8 fb^{-1}. The analysis is very similar to that described in Ref. [9]. The search is performed by selecting events with a dedicated trigger that is used to collect events out-of-time with collisions. The size of the search sample is further reduced by applying a series of offline selection criteria to exclude events that come most likely from our primary sources of background.

The results presented here are an improvement upon previous searches conducted by CMS, the most recent of which used 18.6 fb^{-1} of $\sqrt{s} = 8$ TeV pp collision data taken during 2012 [9] that excluded a gluino with mass below 880 GeV, as well as a stop with mass below 470 GeV.

2 The CMS Detector and Datasets

The central feature of the CMS apparatus is a superconducting solenoid of 6 m internal diameter, providing a magnetic field of 3.8 T. Within the superconducting solenoid volume are a silicon pixel and strip tracker, a lead tungstate crystal electromagnetic calorimeter (ECAL), and a brass and scintillator hadron calorimeter (HCAL), each composed of a barrel and two endcap sections. Forward calorimeters extend the pseudorapidity coverage provided by the barrel and endcap detectors. Muons are measured in gas-ionization detectors embedded in the steel flux-return yoke outside the solenoid. Muons are measured in the pseudorapidity range $|\eta| < 2.4$, with detection planes made using three technologies: drift tubes (DTs) in the barrel, cathode strip chambers (CSCs) in the endcaps, and resistive plate chambers (RPCs) in both the barrel and the endcaps. All these technologies provide both position and timing information. The first level (L1) of the CMS trigger system, composed of custom hardware processors, uses information from the calorimeters and muon detectors to select the most interesting events in a fixed time interval of less than 4 μs. The high-level trigger (HLT) processor farm further de-

creases the event rate from around 100 kHz to less than 1 kHz, before data storage. A more detailed description of the CMS detector, together with a definition of the coordinate system used and the relevant kinematic variables, can be found in Ref. [10].

The search is performed over $\sqrt{s} = 13$ TeV pp collision run data, collected by CMS in 2015 and 2016. The 2015 search sample, taken between August and November 2015, has an integrated luminosity of 2.7 fb^{-1} and corresponds to a trigger livetime of 135 hours. The 2016 search sample is taken between May and October 2016, during which 36.8 fb^{-1} of data were recorded, corresponding to a trigger livetime of 586 hours. In the 2015 search, we use 2015 cosmic run data, collected by our dedicated trigger as our control sample, while 2016 cosmic run data is used in the 2016 search. These dedicated cosmic run data were taken when there were no LHC beams. These control samples, which are signal free and halo free, are used to extrapolate our instrumental noise background.

3 Monte Carlo Simulation

The Monte Carlo simulation is done in three stages. In the first stage, the gluino and stop R-hadrons are produced at the interaction point using PYTHIA 8.205 [11] and then their passage through the detector is simulated by GEANT4 [12]. In case a R-hadron comes at rest in the detector, the particle type and stopping position of the R-hadron are recorded and used as input for the next stage. In this stage, a "cloud model" of R-hadron interactions with the material of the CMS detector is assumed in the simulation. In this model, R-hadrons are treated as supersymmetric particles surrounded by a cloud of loosely bounded quarks or gluons.

In the second stage, those stopped R-hadrons are placed at their stopping points in PYTHIA 6 [13] and their decays are simulated by a second GEANT4 step. In this analysis, the signal samples we used are gluino decays: $\tilde{g} \to g\tilde{\chi}^0$, and stop decays: $\tilde{t} \to t\tilde{\chi}^0$. Two important parameters, stopping efficiency ($\varepsilon_{\text{stopping}}$) and reconstruction efficiency ($\varepsilon_{\text{reco}}$), are derived from the first stage and the second stage respectively. In the end, we perform the third stage toy Monte Carlo simulation. In this stage, we generate toy stopped events in each lumi section (LS) and count the percentage of the subsequent decays taking place within our search window when our trigger is live. We define the effective luminosity (L_{eff}) to be the weighted sum of integrated luminosities in each LS, assuming the weights are the values of the percentage just calculated.

4 Event Selection

We perform the search with a dedicated trigger used to select events out-of-time with respect to collisions. The LHC beams are composed of circulating bunches of protons. In the experiment, bunch crossings (BX) occur nominally at intervals of 25 ns. Although in 2015 and 2016 the bunches of protons are spaced with a 25 ns minimum interval, there are still BXs where there are no bunches of protons passing through. Our trigger selects events at least two BXs away from any proton bunches passing the detector. Furthermore, the trigger requires the events to have at least one jet with energy greater than 50 GeV.

Additional event selection is performed using offline selection criteria to remove our primary backgrounds: halo muons, cosmic muons, and instrumental noise; as well as secondary backgrounds: out of time pp collisions and beam gas. The out of time pp collisions come from rare residual protons between proton bunches. And the beam gas event is induced when a proton strikes the beam pipe inside the detector. To remove these secondary backgrounds we veto the

events that have any reconstructed vertices.

To select events in which the R-hadron decays in the most sensitive instrumented regions, we require that a calorimeter-based jet with an energy of at least 70 GeV is reconstructed. The calorimeter-based jets are reconstructed using an anti-kt clustering algorithm [14] with a distance parameter of 0.4.

Halo muons are one of the primary sources of background for this analysis. They are produced when the proton bunches are diffuse enough to strike the beam pipe or other uninstrumented structures of the LHC. The resulting collision between the proton and the structure produces a shower of particles, most of which decay before reaching the CMS detector. However, the lifetime of muons is long enough for them to traverse the detector. These muons can emit via Bremsstrahlung photons that strike the calorimeters and can be reconstructed as a jet with a large enough energy to be included in our search sample. Since halo muons move primarily along the beam pipe, we remove these events by vetoing the events in which there are any segments having at least 5 reconstructed hits within the CSCs of the muon detector. The high hits multiplicity requirement enables us to increase the $\varepsilon_{\text{neutronCSC}}$ (see Section 5), since unlike those from halo muons, most of the CSC segments from thermal neutrons have less than 5 hits.

Cosmic rays incident on the CMS detector are also a large source of background. Similar to the halo muons, cosmic muons may also emit via Bremsstrahlung photons that strike the calorimeters, leaving large energy deposits. Since cosmic rays feature a large number of reconstructed DT segments and RPC hits, there are some key differences we can exploit to differentiate between signals and cosmic rays. While it is possible for the hadronic shower of R-hadron decay to pass through the first layers of the iron yoke and induce reconstructed DT segments, these DT segments are only located in the inner layers of muon chambers ($R < 560$ cm) and clustered near the leading jet. On the other hand, cosmic rays are equally likely to leave DT segments in all layers in both the upper and lower hemispheres of the muon system, and the angle between the jet and DT segments in ϕ are more evenly distributed. As a result, we are able to substantially reduce the cosmic background contamination in our signal region by rejecting events that have at least two DT segments in the outermost barrel station of the muon system, events that have DT segments in the second outermost barrel station, events having opposite DT segments pairs ($\Delta\phi > \frac{\pi}{2}$), and events with DT segments in the three innermost stations that are far enough from the leading jet in distance of more than 1.0 radians in ϕ. DT segments in the outermost station are more tolerable since we found that signals are very likely to coincide with standalone DT segments that are not from cosmic muons but from proton bunches, and most of these DT segments are located in the outermost muon barrel station. By putting looser requirements on these DT segments from the outermost station, we are able to increase the $\varepsilon_{\text{muonChamber}}$ (see Section 5), thus improving $\varepsilon_{\text{signal}}$ while still rejecting most of the cosmic ray events.

Random electronic noise in the HCAL gives rise to events in which the time response of HCAL readout is very different from the well defined response from particles showering in the calorimeter. These HCAL readouts could lead to spurious clustered energy deposits that can be reconstructed as a jet, thus contaminating our signal region and needs to be rejected. The HCAL readout is analog signal pulses over ten BXs centered around the pulse maximum. The pulse shape from showering particles features a clear centered peak and an exponential decay over the subsequent BXs. We use a series of offline selection criteria that exploit these timing and topological characteristics to remove the HCAL noise events. These criteria are described in detail in Ref. [15].

By applying these dedicated background veto selection criteria, we are able to reject most of

Table 1: Summary of $\varepsilon_{\text{signal}}$ for different signals.

	2015 gluino	2015 stop	2016 gluino	2016 stop
$\varepsilon_{\text{stopping}}$	5.4%	4.5%	5.4%	4.5%
$\varepsilon_{\text{reco}}$	47.2%	35.5%	53.3%	39.9%
$\varepsilon_{\text{neutronCSC}}$	98.0%	98.0%	94.4%	94.4%
$\varepsilon_{\text{muonChamber}}$	97.7%	97.7%	87.7%	87.7%
ε_{signal}	2.5%	1.8%	2.3%	1.4 %

the background events.

5 Signal Efficiency

In this section we describe the calculation of the signal efficiency ($\varepsilon_{\text{signal}}$), which is defined as the product of $\varepsilon_{\text{stopping}}$, $\varepsilon_{\text{reco}}$, $\varepsilon_{\text{neutronCSC}}$ and $\varepsilon_{\text{muonChamber}}$.

In the first stage of the simulation, the R-hadrons interact with detector material through a combination of ionization and nuclear interaction. The R-hadrons are most likely to come at rest in the densest part of the detector, such as the HCAL and ECAL. This analysis concentrates on the HCAL barrel (HB) and ECAL barrel (EB) regions, where there is less background and the decay of R-hadrons will leave a cluster of HCAL and ECAL deposits, having a unique detector signature of single jet. The R-hadrons could also stop within the iron yokes interleaved with the muon detector system, but a decay producing a jet is unlikely to be observed. The number of R-hadrons that stop in the tracker is negligible.

We define the stopping efficiency as the probability of a first stage event to have a R-hadron stopped in the HB or EB. After the first stage simulation, we get $\varepsilon_{\text{stopping}} \approx 5\%$ for gluinos and $\varepsilon_{\text{stopping}} \approx 4\%$ for stops. The efficiency is lower than that in the 2012 search due to the increase of the center of mass energy.

The reconstruction efficiency ($\varepsilon_{\text{reco}}$) is defined as the number of events that pass our full offline selection criteria divided by the number of signal events that stop within the barrel region of the calorimeter, assuming that all decays happen in our search window when the trigger is live. We assume BR($\tilde{g} \to g\tilde{\chi}^0$) = 100% and BR($\tilde{t} \to t\tilde{\chi}^0$) = 100%. $\varepsilon_{\text{reco}}$ depends primarily on the energy of visible daughter particle of the R-hadron decay, E_{g} (E_{t}). Above the minimum energy threshold, $E_{\text{g}} > 130$ GeV ($E_{\text{t}} > 170$ GeV), $\varepsilon_{\text{reco}}$ becomes approximately constant, as shown in Fig. 1. The $\varepsilon_{\text{reco}}$ of 2016 analysis is different than that in the 2015 analysis, since the beam halo filter is removed in the trigger of 2016. At the plateau, $\varepsilon_{\text{reco}}$ is 47% (35%) for $\tilde{g}$ ($\tilde{t}$) decays in the 2015 analysis, and 53% (40%) for $\tilde{g}$ ($\tilde{t}$) decays in the 2016 analysis.

In the CMS detector, it is possible for a signal to coincide with DT segments or CSC segments that originate from effects not modeled in the simulation. One example is thermal neutrons, which have a long time-of-flight and could take as long as a tenth of a second after being produced in pp collisions until they arrive at the muon chambers and induce CSC or DT segments. These segments could occur when there are no bunch crossings, and thus it is likely that some of the events in our search sample contain these additional segments originating from the proton bunches. To prevent the signal efficiency being overestimated, we add $\varepsilon_{\text{neutronCSC}}$ ($\varepsilon_{\text{muonChamber}}$) into our signal efficiency to take into account the degradation of signal efficiency due to these extra CSC or DT segments in the detector.

The $\varepsilon_{\text{neutronCSC}}$ ($\varepsilon_{\text{muonChamber}}$) is defined as the ratio of the probability that a signal passes the

beam halo (cosmic ray) rejection criteria in data to the probability that a signal passes the same criteria in the simulation. HCAL noise events are good candidates for estimating these two efficiencies from data, since the noise is independent of any muon chamber activities and should pass both beam halo rejection and cosmic ray rejection criteria. These events are selected by inverting a few of the noise rejection criteria. Then $\varepsilon_{\text{neutronCSC}}$ ($\varepsilon_{\text{muonChamber}}$) is simply the percentage of noise events that pass the beam halo (cosmic ray) rejection criteria among all selected noise events. Table 1 summarizes the values of $\varepsilon_{\text{neutronCSC}}$ and $\varepsilon_{\text{muonChamber}}$ for different signals.

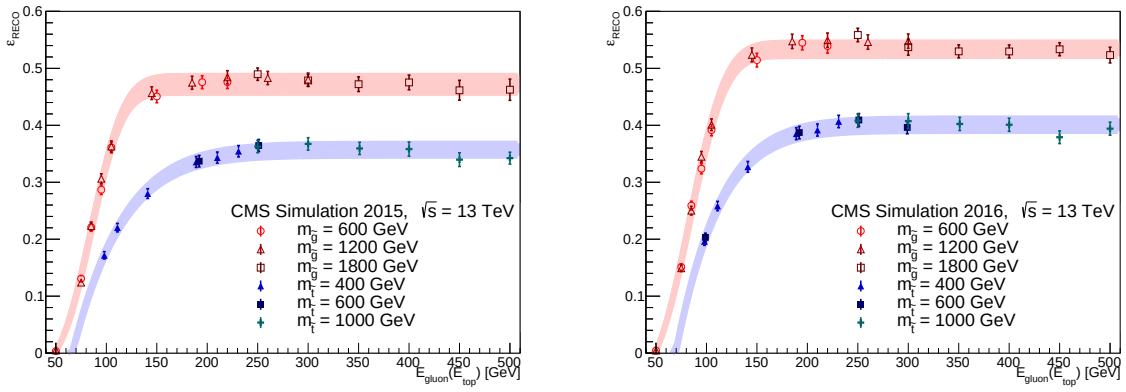

Figure 1: $\varepsilon_{\text{reco}}$ for $\tilde{g}$ and $\tilde{t}$ R-hadrons that stopped in the EB or HB as a function of energy of the SM daughter particle. The left plot corresponds to the 2015 MC simulation and the right one corresponds to the 2016 MC simulation. The difference between the two plots is due to the removal of the beam halo filter in the trigger in 2016. The shaded areas correspond to the systematic uncertainties, which are described in Section 7.

6 Background estimation

The inefficiencies of each of the primary background vetoes are calculated as follows. These inefficiencies represent the probability of background events escaping the background veto and thus being observed by our search.

It is possible for halo muons to escape detection in the endcaps of the muon system. Although escaping detection is extremely rare, due to the high rate of halo events in 2015 and 2016, the halo background is non-negligible. We estimate the halo veto inefficiency using a data-driven "tag-and-probe" method that analyzes a high-purity sample of halo events by selecting events that have CSC segments in at least two endcap layers of muon system. The events are first classified according to their origin of clockwise or counterclockwise beam. Then for each class, depending on whether these events have CSC segments in only one endcap or both endcaps of the muon system, they are categorized into events that have only "incoming" portion of halo muon track, events that have only "outgoing" portion and events that have "both" portions. Then the number of events that escape the detection can be estimated as $\frac{N_{\text{IncomingOnly}} \times N_{\text{OutgoingOnly}}}{N_{\text{Both}}}$. After binning halo events according to their geometrical location and performing the classification and calculation discussed above, the halo veto inefficiency is estimated to be $\sim 1 \times 10^{-4}$. The efficiency is then multiplied by the halo events vetoed in the search region where cosmic and noise vetoes are already applied, yielding a halo background estimate of 1.1 ± 0.1 events for 2015 analysis and 2.6 ± 0.2 for 2016 analysis.

To determine the rate at which cosmic muons escape detection by the cosmic muon veto, we generate a sample of 60 million simulated cosmic events using CMSCGEN [16], which is based on the air shower program CORSIKA [17], and has been validated in [18]. Out of 60 million cosmic events, 54k events meet the requirement of the minimum selection criteria, which require substantial deposits in the calorimeters and no CSC segments in the muon endcap system that would cause the event to be classified as a halo muon.

Using these 54k signal-like simulated cosmic events, the cosmic veto inefficiency is then estimated by dividing the number of simulated cosmic events that escape the cosmic veto by the total number of cosmic events. Out of these 54k simulated cosmic events, 137 events pass the cosmic veto criteria, thus we expect our cosmic veto inefficiency to be $\sim 1 \times 10^{-3}$. To account for the small difference in occupancy between the cosmic data and MC simulation, we bin the events in the number of DT and outer barrel RPC hits. This inefficiency is then multiplied in each bin by the number of cosmic events vetoed in the search region where halo veto and noise vetoes are already applied. The integration of the result gives a cosmic background of 2.6 ± 0.9 events for 2015 analysis, and that of 8.8 ± 3.1 for 2016 analysis.

Finally, the background estimation of instrumental noise is performed using control data in cosmic runs, which are runs with no beams in the LHC thus including only cosmic events and noise events. After applying all selection criteria on the control data, we observed 2 events in the 2015 control data and 2 events in the 2016 control data. We then subtract the cosmic background from the total event yield, getting a noise background estimate of $0.3^{+2.4}_{-0.3}$ events (2015 control data) and $0.0^{+2.2}_{-0.0}$ (2016 control data). Based on the number of noise events in the control sample, we expect the noise veto inefficiency to be $\leq 1 \times 10^{-4}$. These noise estimates are then scaled to the search data, assuming that the noise veto inefficiency remains the same. The resultant noise background estimate is $0.4^{+2.9}_{-0.4}$ for the 2015 analysis and $0.0^{+9.8}_{-0.0}$ events for the 2016 analysis. The uncertainty in the 2016 analysis is large because in 2016 the duration of cosmic runs was much shorter than that of collision runs.

In summary, the total background estimate of 2015 is $4.1^{+3.0}_{-1.0}$ events, while that of 2016 is $11.4^{+10.3}_{-3.1}$ events, as summarized in Table 3.

7 Sources of Systematic Uncertainty

The systematic uncertainty due to trigger efficiency is negligible since the offline jet energy criterion ensures the data analyzed are well above the turn-on region, where the $\varepsilon_{\text{reco}}$ becomes constant. The uncertainty on the luminosity is estimated within 2.3% for the 2015 data and within 2.5% for the 2016 data [19, 20]. The uncertainty of $\varepsilon_{\text{reco}}$ is estimated to be $\delta_{\varepsilon_{\text{reco}}} = 7.7\%(5.2\%)$ for $\tilde{g}(\tilde{t})$ in the 2015 analysis, and $\delta_{\varepsilon_{\text{reco}}} = 7.5\%(5.2\%)$ for $\tilde{g}(\tilde{t})$ in the 2016 analysis. This uncertainty is determined by computing the maximal relative difference between $\varepsilon_{\text{reco}}$ of points on the plateau and the value of $\varepsilon_{\text{reco}}$ listed in Table 1. The shaded bands in Fig. 1 describe this uncertainty.

Jets in this analysis are not formed by particles originating from the center of the detector, so the standard uncertainty of the jet energy scale (JES) does not apply. Instead, we refer to a study performed on the HCAL during cosmic data taking in 2008 [21]. This study compares the energy of the reconstructed jets in simulated cosmic ray events and cosmic ray events in data, concluding that the uncertainty of jet energy in the simulation is $\sim$ 2%. Moreover, a study conducted with 2012 data [22] compares the data and simulation for dijets originating from the interaction point. The comparison leads to an estimate of $<$ 2% for jets striking the HCAL barrel with angles of incidence from 0 to 60 degrees. By assuming that the jet energy scale is

2%, the uncertainty of the signal efficiency is expected to be 2%. This estimate is conservative since only the yield of signals with jet energy around the offline threshold is affected by the variation of the jet energy, and as a result the uncertainty decreases rapidly as E_g (E_t) increases.

The total signal systematic uncertainty on the signal yield is 8.3% in the 2015 search, while in the 2016 search, the uncertainty is 8.2%. The systematic uncertainties are summarized in Table 2.

Table 2: The systematic uncertainties in the 2015 and 2016 searches.

	2015 search data	2016 search data
Reconstruction Efficiency	7.7%	7.5%
Luminosity	2.3%	2.5%
JES	2.0%	2.0%
total syst. uncertainty	8.3%	8.2%

8 Search Results and 95% CL Exclusion Limits on Gluino and Stop Production

The search results are shown in Table 3. Four events are observed in the 2015 analysis and thirteen events are observed in the 2016 analysis. Both observed numbers of events are consistent with the predicted backgrounds.

Table 3: Summary of background predictions and search results for the 2015/2016 search.

Period	Livetime (hrs)	Noise	Cosmics	Halo	Total	Observed
2015 control	-	$0.3^{+2.4}_{-0.3}$	1.7 ± 0.6	0	-	2
2015	135	$0.4^{+2.9}_{-0.4}$	2.6 ± 0.9	1.1 ± 0.1	$4.1^{+3.0}_{-1.0}$ (the median is 6.2)	4
2016 control	-	$0^{+2.2}_{-0}$	2.5 ± 0.9	0	-	2
2016	586	$0^{+9.8}_{-0}$	8.8 ± 3.1	2.6 ± 0.2	$11.4^{+10.3}_{-3.1}$ (the median is 17.4)	13

We perform a counting experiment in equally spaced $\log_{10}(\text{time})$ bins of gluino lifetime hypotheses from 10^{-7} to 10^{6} seconds. For lifetime hypotheses shorter than one orbit (89 μs), we count only candidates within a sensitivity-optimized time window of $1.3\tau_{\tilde{g}}$ from any pp collision. This restriction avoids the addition of backgrounds for time intervals during which the signal has a high probability to have already decayed. We assume that the cosmic and noise backgrounds are uniformly distributed in time, and estimate the halo background in each lifetime hypothesis by counting the ratio of halo events in the search time window ($1.3\tau_{\tilde{g}}$) to the total number of halo events, then multiplying this ratio by the halo background estimate at full trigger livetime. For lifetimes smaller than one orbit, both the number of observed events and the expected background depend on the time window considered, which is a fraction of the total trigger livetime. Similarly, the effective luminosity is smaller than the maximum for short lifetimes. As we gradually increase the lifetime in the hypothesis from the minimal value, we include more observed events in our search window. In the lifetime region where the lifetime is smaller than a single orbit, to explicitly show the discontinuous changes of the upper limits whenever our expanding search window covers a new observed event, we test two additional lifetime hypotheses for each observed event for these counting experiments: The largest lifetime hypothesis for which the event lies outside $1.3\tau_{\tilde{g}}$, and the smallest lifetime hypothesis for which the event is contained within $1.3\tau_{\tilde{g}}$. For lifetimes bigger than a single orbit, the trigger livetime, the expected background, and the number of observed events are independent of the lifetime. The effective luminosity decreases with lifetimes after the lifetimes are longer than one LHC fill. Table 4 shows the results of the counting experiment.

Table 4: Results of the 2016 counting experiments for selected lifetime hypotheses.

Lifetime	$L_{eff}(fb^{-1})$	Livetime (s)	Expected bkg	Observed
50 ns	0.27	6.2×10^4	$0.4^{+0.3}_{-0.1}$	0
75 ns	0.65	12.3×10^4	$0.8^{+0.6}_{-0.2}$	0
100 ns	1.27	2.4×10^5	$1.4^{+1.2}_{-0.4}$	0
1 μs	9.98	1.5×10^6	$8.4^{+7.5}_{-2.3}$	8
10 μs	13.37	2.1×10^6	$11.3^{+10.2}_{-3.1}$	13
100 μs	13.70	2.1×10^6	$11.4^{+10.3}_{-3.1}$	13
10^3 s	13.57	2.1×10^6	$11.4^{+10.3}_{-3.1}$	13
10^4 s	11.78	2.1×10^6	$11.4^{+10.3}_{-3.1}$	13
10^5 s	8.27	2.1×10^6	$11.4^{+10.3}_{-3.1}$	13
10^6 s	5.61	2.1×10^6	$11.4^{+10.3}_{-3.1}$	13

By combining the likelihoods of search results from the 2015 and 2016 analyses, and assuming $E_g > 130$ GeV ($E_t > 170$ GeV), we are able to set combined limits on the $\sigma \times BR$ (see Fig. 2) of $\tilde{g}(\tilde{t})$ pair production. As a result, we can exclude $m_{\tilde{g}} < 1385$ GeV and $m_{\tilde{t}} < 744$ GeV at 95% CL for 10 μs $< \tau <$ 1000 s (see Fig. 3) . A hybrid CLs method is used in limit setting to incorporate the systematic uncertainties.

Accordingly, Figure 4 shows the regions of the gluino mass/ neutralino mass plane excluded by the combined analysis, for lifetimes between 10 μs and 1000s. Figure 5 shows the same except for the stop mass/ neutralino mass plane.

9 Conclusion

A search has been made for long-lived particles that have stopped in the CMS detector after being produced in 13 TeV pp collisions at the CERN LHC. The subsequent decays of these particles were looked for during gaps between proton bunches in the LHC beams. In 2.7 fb^{-1} of 13 TeV pp collision run data, with a search interval corresponding to 135 hours of trigger livetime in 2015 and 36.8 fb^{-1} of 13 TeV pp collision run data collected in a search interval of 586 hours of trigger livetime for 2016, no excess above the estimated background was observed. Cross section and mass limits are presented at 95% CL on gluino and stop production over 13 orders of magnitude in the mean proper lifetime of the stopped particle. Assuming a cloud model of R-hadron interactions, and combining the results from the 2015 and 2016 analyses, for $E_g > 130$ GeV and $BR(\tilde{g} \to g\tilde{\chi}^0) = 100\%$, gluinos with lifetimes from 10 μs to 1000s and $m_{\tilde{g}} < 1385$ GeV are excluded. Under a similar assumption, $E_t > 170$ GeV and $BR(\tilde{t} \to t\tilde{\chi}^0) = 100\%$, we are able to exclude long-lived stop quarks with lifetimes from 10 μs to 1000s and $m_{\tilde{t}} < 744$ GeV. These are the strongest limits on stopped long-lived particles to date.

References

[1] S. Dimopoulos, M. Dine, S. Raby, and S. D. Thomas, "Experimental signatures of low-energy gauge mediated supersymmetry breaking", *Phys. Rev. Lett.* **76** (1996) 3494–3497, doi:10.1103/PhysRevLett.76.3494, arXiv:hep-ph/9601367.

[2] H. Baer, K.-m. Cheung, and J. F. Gunion, "A Heavy gluino as the lightest supersymmetric particle", *Phys. Rev.* **D59** (1999) 075002, doi:10.1103/PhysRevD.59.075002, arXiv:hep-ph/9806361.

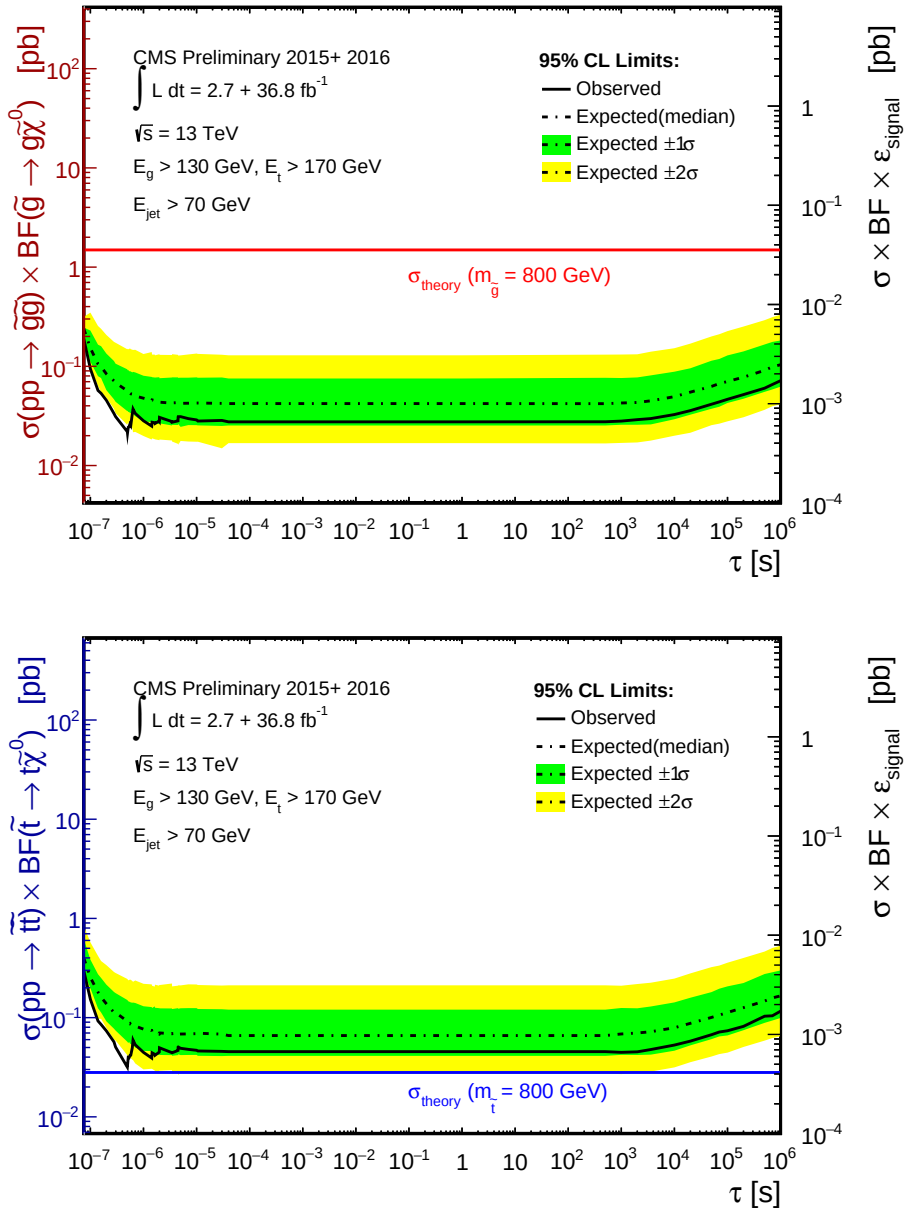

Figure 2: Combined expected and observed 95% CL limits on gluino and stop pair production cross section (left-hand axes) using the cloud model of R-hadron interactions, as a function of particle lifetime. The discontinuous structure observed between 10^{-7} s and 10^{-5} s is due to the increase of the number of observed events in our search window as lifetime increases.

[3] T. Jittoh, J. Sato, T. Shimomura, and M. Yamanaka, "Long life stau in the minimal supersymmetric standard model", *Phys. Rev.* **D73** (2006) 055009, doi:10.1103/PhysRevD.73.055009,10.1103/PhysRevD.87.019901, arXiv:hep-ph/0512197. [Erratum: Phys. Rev.D87,no.1,019901(2013)].

[4] M. J. Strassler and K. M. Zurek, "Echoes of a hidden valley at hadron colliders", *Phys. Lett.* **B651** (2007) 374–379, doi:10.1016/j.physletb.2007.06.055, arXiv:hep-ph/0604261.

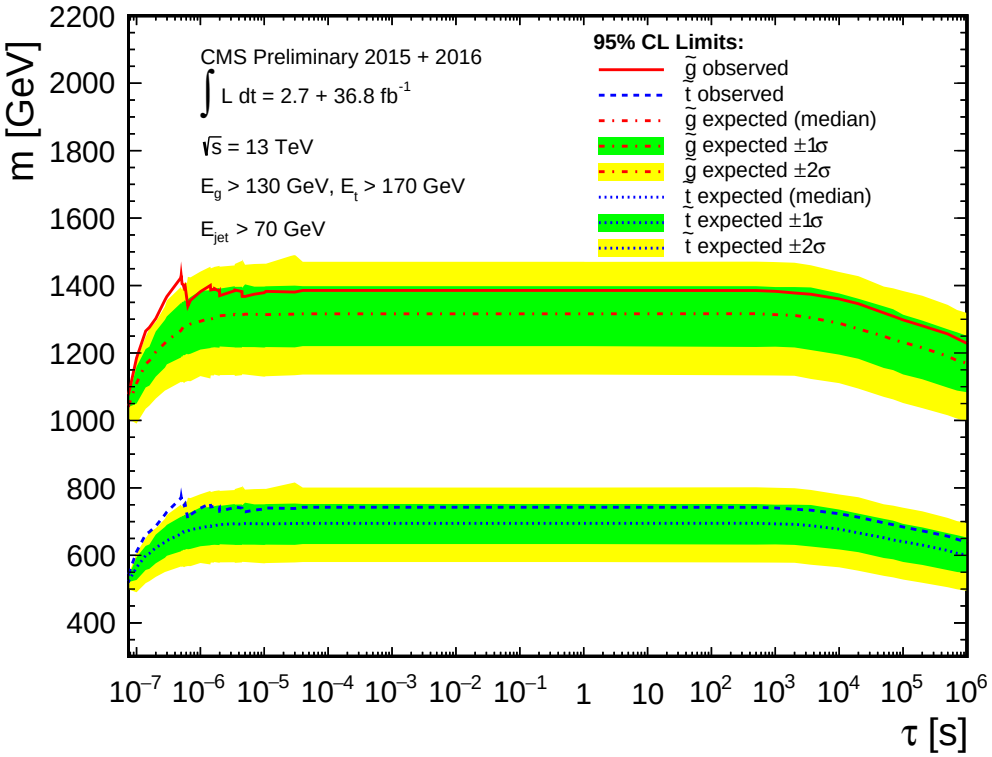

Figure 3: Combined expected and observed 95% CL limits on gluino and stop mass using the cloud model of R-hadron interactions, as a function of particle lifetime. The discontinuous structure observed between 10^{-7} s and 10^{-5} s is due to the increase of the number of observed events in our search window as lifetime increases.

[5] A. Arvanitaki et al., "Astrophysical Probes of Unification", *Phys. Rev.* **D79** (2009) 105022, doi:10.1103/PhysRevD.79.105022, arXiv:0812.2075.

[6] N. Arkani-Hamed and S. Dimopoulos, "Supersymmetric unification without low energy supersymmetry and signatures for fine-tuning at the LHC", *JHEP* **06** (2005) 073, doi:10.1088/1126-6708/2005/06/073, arXiv:hep-th/0405159.

[7] CMS Collaboration, "Search for long-lived charged particles in proton-proton collisions at $\sqrt{s} = 13$TeV", *Phys. Rev.* **D94** (2016), no. 11, 112004, doi:10.1103/PhysRevD.94.112004, arXiv:1609.08382.

[8] ATLAS Collaboration, "Search for heavy long-lived charged *R*-hadrons with the ATLAS detector in 3.2 fb^{-1} of proton–proton collision data at $\sqrt{s} = 13$ TeV", *Phys. Lett.* **B760** (2016) 647–665, doi:10.1016/j.physletb.2016.07.042, arXiv:1606.05129.

[9] CMS Collaboration, "Search for decays of stopped long-lived particles produced in proton-proton collisions at $\sqrt{s} = 8$ TeV", *Eur. Phys. J.* **C75** (2015) 151, doi:10.1140/epjc/s10052-015-3367-z, arXiv:1501.05603.

[10] CMS Collaboration, "The CMS experiment at the CERN LHC", *JINST* **3** (2008) S08004, doi:10.1088/1748-0221/3/08/S08004.

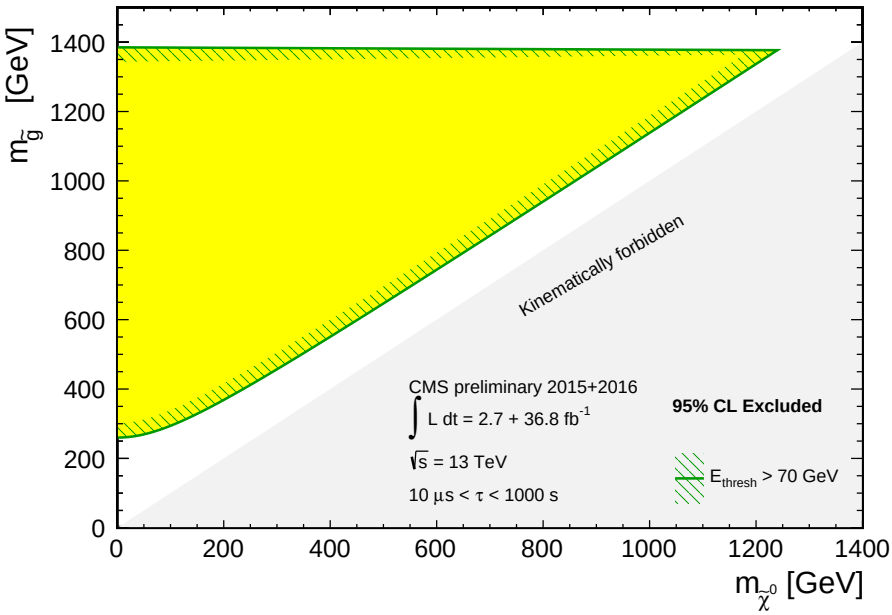

Figure 4: Combined observed 95% CL limits in the gluino mass/ neutralino mass plane, for lifetimes between 10 μs and 1000s

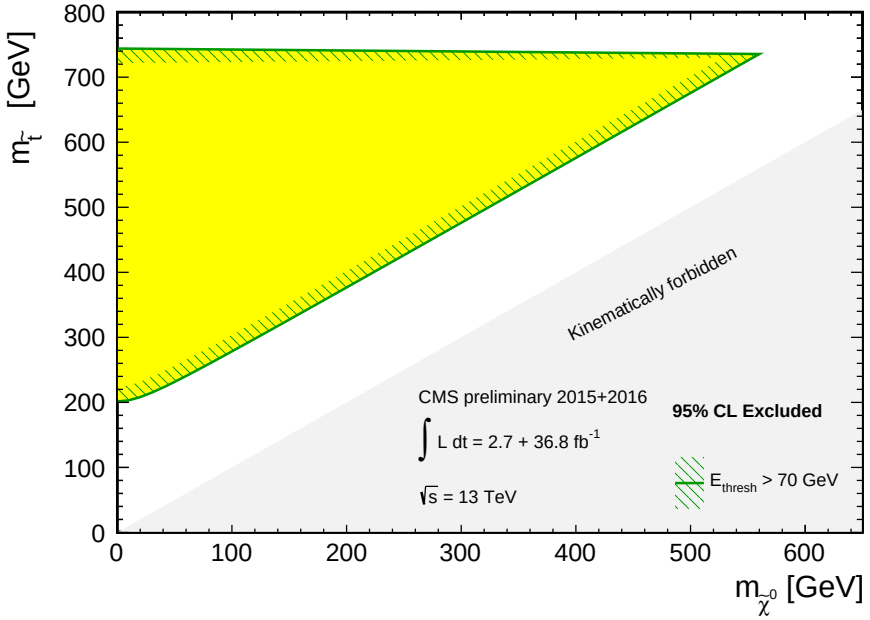

Figure 5: Combined observed 95% CL limits in the stop mass/ neutralino mass plane, for lifetimes between 10 μs and 1000s

[11] T. Sjostrand, S. Mrenna, and P. Z. Skands, "A Brief Introduction to PYTHIA 8.1", *Comput. Phys. Commun.* **178** (2008) 852–867, doi:10.1016/j.cpc.2008.01.036, arXiv:0710.3820.

[12] GEANT4 Collaboration, "GEANT4: A Simulation toolkit", *Nucl. Instrum. Meth.* **A506**

(2003) 250–303, doi:10.1016/S0168-9002(03)01368-8.

[13] T. Sjöstrand, S. Mrenna, and P. Skands, "PYTHIA 6.4 physics and manual", *JHEP* **05** (2006) 026, doi:10.1088/1126-6708/2006/05/026, arXiv:hep-ph/0603175.

[14] M. Cacciari, G. P. Salam, and G. Soyez, "The anti-k_t jet clustering algorithm", *JHEP* **04** (2008) 063, doi:10.1088/1126-6708/2008/04/063, arXiv:0802.1189.

[15] CMS Collaboration, "Search for Stopped Gluinos in pp collisions at $\sqrt{s} = 7$ TeV", *Phys. Rev. Lett.* **106** (2011) 011801, doi:10.1103/PhysRevLett.106.011801, arXiv:1011.5861.

[16] P. Biallass and T. Hebbeker, "Parametrization of the Cosmic Muon Flux for the Generator CMSCGEN", arXiv:0907.5514.

[17] D. Heck et al., "CORSIKA: A Monte Carlo code to simulate extensive air showers",.

[18] CMS Collaboration, G. Hesketh, "Measurement of the Charge Ratio of Atmospheric Muons with the CMS Detector", in *Proceedings, 16th International Symposium on Very High Energy Cosmic Ray Interactions (ISVHECRI 2010)*. 2010. arXiv:1009.1036.

[19] CMS Collaboration, "CMS Luminosity Measurement for the 2015 Data Taking Period", *CMS Physics Analysis Summary* **CMS-PAS-LUM-15-001** (2016).

[20] CMS Collaboration, "CMS Luminosity Measurements for the 2016 Data Taking Period", *CMS Physics Analysis Summary* **CMS-PAS-LUM-17-001** (2017).

[21] CMS Collaboration, "Performance of the CMS hadron calorimeter with cosmic ray muons and LHC beam data", *Journal of Instrumentation* **5** (2010), no. 03, T03012.

[22] CMS Collaboration, "Performance of jets at CMS", *Journal of Physics: Conference Series* **587** (2015), no. 1, 012004.